The leading-edge drag was computed by summing the forces from the modified Newtonian expression for the local pressure coefficient. For equal inner and outer θ_j value, see Fig. 1:

$$C_{D,b} = 4C_{p,t,2}(d/D_c)(\sin\theta_j)(1 - \tfrac{1}{3}\sin^2\theta_j)$$

For θ_j of 90°, this reduces to

$$C_{D,b} = \tfrac{8}{3}C_{p,t,2}(d/D_c)$$

Rounding the leading edges would raise the pressures on the outer surface. Figure 3 of Ref. 2 provides means for obtaining a two-dimensional approximation for these pressures. Pressure coefficients were integrated over the outer conical surface to obtain corresponding drag coefficients.

For purposes of this study a value of the hypersonic similarity parameter, $\tan\delta(M_\infty^2 - 1)^{1/2}$, of 0.3116 was used and a ratio of exit area to capture area of 3 was assumed. These assumptions produce slender bodies that increase in length as M_∞ increases.

The results of the outer-surface pressure-drag coefficient and the total external pressure-drag coefficient calculations are shown in Fig. 1. The curves show that the leading-edge drag coefficient is high for even small amounts of leading-edge rounding. The effect of leading-edge bluntness on the outer-surface pressure-drag coefficient is minor. For even modest amounts of leading-edge rounding the leading-edge drag is the major portion of the total drag.

The high pressure drag of blunted leading edges may be reduced significantly by sweeping the leading edge; for instance, a rectangular inlet might be incorporated in the swept leading edge of a wing. An analysis was made of a unit length of leading edges and considered only the upper and lower leading edges. The upper and lower circular leading edges were assumed followed by flat surfaces parallel to the freestream. This simplification does not affect the leading-edge pressure-drag coefficient strongly and is justified by a lack of knowledge of the final geometry at this point. The analysis gave the expression

$$C_{D,b} = \tfrac{4}{3}(d/g)C_{p,t,\beta}\cos^2\beta$$

The effect of sweep angle on leading-edge drag coefficient is given in Fig. 2 for freestream Mach numbers of 12 and 15; increasing M_∞ from 12 to 15 produced no significant effect on $C_{D,b}$. No consideration of the end boundaries of the rectangular inlets was made. It is probable with long rectangular inlets that intermediate vertical partitions would be required for structural and/or internal-flow considerations. Sweeping the leading edge from 0° to 70° reduced the drag coefficient by a factor of about 10.

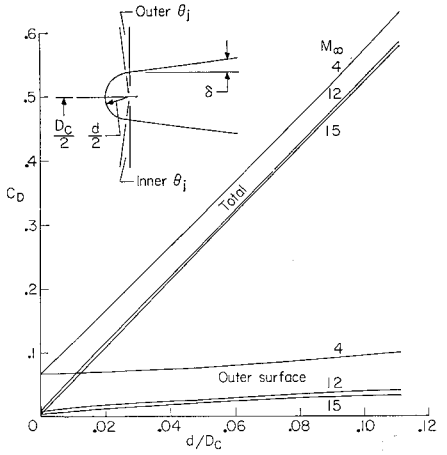

Fig. 1 External pressure-drag breakdown; circular inlets; exit area to capture area ratio 3; $\tan\delta(M_\infty^2 - 1)^{1/2}$, 0.3116; perfect gas.

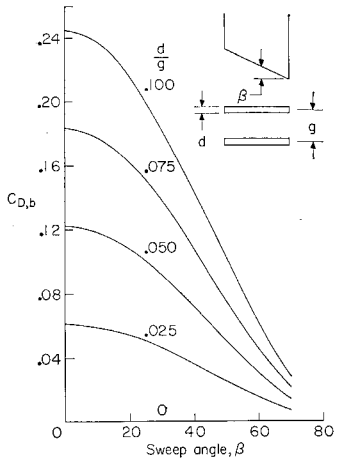

Fig. 2 Leading edge pressure-drag coefficient; semicircular leading edges; modified Newtonian theory; perfect gas; $M_\infty = 12$, $M_\infty = 15$.

In conclusion estimates have shown the increase in total external pressure drag caused by rounding the leading edges of conical ducted bodies to be considerable. Consideration of sweeping the leading edges showed possibilities of markedly decreasing the drag penalty deriving from the necessity of having rounded leading edges.

References

[1] Valentine, E. F., "External-drag estimation for slender conical ducted bodies at high Mach numbers and zero angle of attack," NASA TN D-648 (1961).

[2] Baradell, D. L. and Bertram, M. H., "The blunt plate in hypersonic flow," NASA TN D-408 (1961).

Reaction of Hydrazine and Nitrogen Tetroxide in a Low-Pressure Environment

ROBERT A. WASKO*
NASA Lewis Research Center, Cleveland, Ohio

THE use of hypergolic propellants in space vehicle propulsion systems raises questions concerning the effect of a vacuum on the reaction of these propellants.

A preliminary study was made of the reaction of hydrazine and nitrogen tetroxide at pressures as low as 10^{-4} Torr (mm Hg). A steel vacuum tank served as a vessel wherein stoichiometric quantities of these propellants, separately encapsuled in glass tubing under atmospheric pressure and at room temperature, were broken simultaneously (see inset in Fig. 2).

The vacuum tank was 4 ft wide and 6 ft long with one end covered by a glass window for viewing purposes. The capsules were broken by a cleaver device that was remotely actuated by a solenoid release. Temperatures were recorded in the vicinity of the capsules, and tank pressure was measured by an ionization gage and a Pirani gage. High-speed motion pictures also were obtained.

Effects of varying the total propellant quantity on the tank pressure rise are shown in Fig. 1. In all cases, the initial tank pressure was about 4×10^{-4} Torr. With small quantities of propellants (2.3 and 4.6 cm³), the pressure rose to a value predicted from perfect gas equations for complete

Received May 10, 1963; revision received May 27, 1963.
* Aeronautical Research Engineer. Associate Member AIAA.

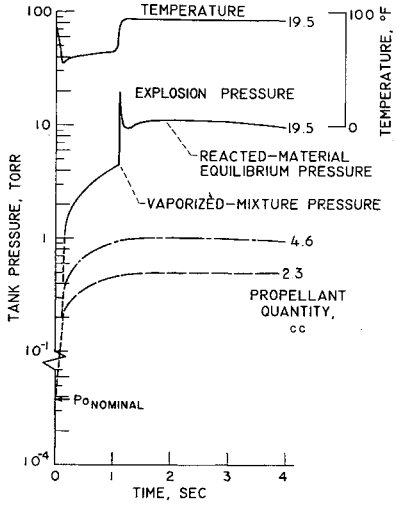

Fig. 1 Effect of varying propellant quantity on tank pressure rise.

propellant vaporization, which indicates that there was no reaction. With larger quantities of propellants (19.5 cm³), the initial pressure rise (to the "vaporized-mixture-pressure" point) again could be predicted with complete vaporization assumed. This pressure rise was followed by an explosion pressure fluctuation that occurred when the tank pressure exceeded 4 Torr. The tank pressure ultimately reached a new equilibrium value. As expected, the transient temperature variations show a sharp decrease during propellant vaporization and a sharp rise during the reaction phase. The gradual temperature rise in between was caused by radiant energy from photographic flood lamps. It was apparent from the motion-picture film that the magnitude of the temperature decrease was sufficient to cause freezing of droplets of hydrazine on the capsule support mechanism. Later tests with single capsules of either N_2H_4 or N_2O_4 confirmed the fact that this freezing phenomenon occurred only in the N_2H_4.

Figure 2 shows the change in pressure-time history for various initial tank pressures p_0. In all cases, the reaction occurred at vaporized-mixture pressures greater than 4 Torr. Comparison of the three curves indicates a large reaction delay time for $p_0 = 1$ Torr, whereas for $p_0 = 6 \times 10^{-4}$ and 10^{-1} Torr, the reaction occurred after approximately 0.9 sec, and 2.25 sec were required at $p_0 = 1$ Torr. In addition, the sudden increase in pressure associated with explosion did not occur for an initial ambient pressure of 1 Torr; rather, the pressure increased smoothly from the vaporized-mixture to the reacted-material equilibrium pressure. Evidently, the region from 10^{-1} to 1 Torr is a transition region in which a less violent reaction occurs. Increasing ambient pressure increases the amount of inert gas (nitrogen) in the tank; thus the dilution of the propellant may explain this phenomenon.

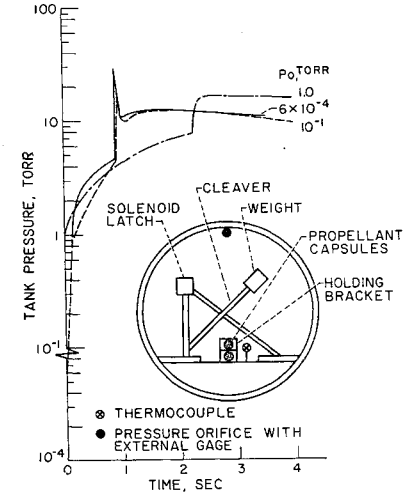

Fig. 2 Tank pressure rise with varying initial pressure; total propellant volume = 19.5 cm³.

Conclusions

1) An explosive reaction occurred only when a sufficient quantity of propellant was used to produce a vaporized mixture pressure greater than 4 Torr.

2) For the decade of initial ambient pressure from 10^{-1} to 1 Torr, the reaction changed from an explosion to a slower reaction, as evidenced by a decrease in the magnitude of the explosion pressure and an increase in the reaction delay time.

3) N_2O_4 vaporized more quickly than N_2H_4, and the temperature decrease due to vaporization was sufficient to cause freezing of a portion of the N_2H_4.

A General Formula for Stiffness Matrices of Structural Elements

G. C. Best
Fort Worth, Texas

In this note a method is shown for developing stiffness matrices of elements composed of continuous elastic material. Following the general plan of Ref. 2, a stress assumption is made and loads are taken as the resultants of these stresses integrated over the sides. In matrix notation the stress assumption can be expressed as

$$\sigma = Uk \tag{1}$$

where $\sigma = \text{col}(\sigma_x,\sigma_y,\sigma_z,\ \tau_{xy},\tau_{yz},\tau_{zx})$ is the stress vector (assuming three dimensions), $k = \text{col}(k_1,\ k_1,\ \ldots k_r)$ with each k a constant, and U is a matrix whose elements are easily integrated functions of x,y,z, (e.g., $x^{v_1}y^{v_2}z^{v_3}$ with the v_i integers or zero) so that each stress is assumed approximated by a linear combination of elementary functions chosen to satisfy the differential equations of equilibrium and the equations of compatibility.

Integrating stresses over the surface of the element yields

$$p = Vk \tag{2}$$

giving a relation between the applied load vector p and the vector k. The elements of V are constants determined by the limits of integration.

Let m be the order of the stiffness matrix of the supported element. The number r of constants in the stress assumption is taken to be greater than m. For any given loading, the constants that are therefore in excess are so adjusted as to minimize the function

$$\overline{W} = \frac{1}{2}\oint_S \bar{\sigma}^T\bar{\sigma}dS \tag{3}$$

where $\bar{\sigma} = \text{col}(\sigma_n,\tau_{n1},\tau_{n2})$ and $\sigma_n,\tau_{n1},\tau_{n2}$ are the normal and shearing stresses on the surface of the element of surface area S. Let the matrix T transform from x,y,z coordinates to surface coordinates. Then

$$\bar{\sigma} = T\sigma \tag{4}$$

Inserting Eqs. (1) and (4) in (3) gives

$$\overline{W} = \frac{1}{2}k^T\left(\oint_S U^TT^TTUdS\right)k = \frac{1}{2}k^TBk \tag{5}$$

where $B = (b_{\alpha,\beta})$, and the parenthesized part in Eq. (5) is an $r \times r$ matrix that can be evaluated by numerical integration.

The minimization of (5) holding the loads constant is an isoperimetric problem in the calculus of variations.[3] Hence

Received May 20, 1963.